Behavior of a porous particle in a radiofrequency plasma under pulsed argon ion beam bombardment

To cite this article: Ruben Wiese *et al* 2010 *New J. Phys.* **12** 033036

View the article online for updates and enhancements.

Behavior of a porous particle in a radiofrequency plasma under pulsed argon ion beam bombardment

Ruben Wiese[1,2], **Vladimir Sushkov**[1], **Holger Kersten**[3], **Venkata R Ikkurthi**[1], **Ralf Schneider**[4] and **Rainer Hippler**[1,5]

[1] Institut für Physik, Ernst-Moritz-Arndt-Universität Greifswald, Felix-Hausdorff-Strasse 6, 17489 Greifswald, Germany
[2] Institut für Plasmaforschung und Technologie, Felix-Hausdorff-Strasse 2, 17489 Greifswald, Germany
[3] Institut für Experimentelle und Angewandte Physik, Universität Kiel, Kiel, Germany
[4] Max-Planck-Institut für Plasmaphysik, EURATOM Association, Wendelsteinstrasse 1, 17491 Greifswald, Germany
E-mail: hippler@physik.uni-greifswald.de

Abstract. The behavior of a single porous particle with a diameter of $250\,\mu$m levitating in a radiofrequency (RF) plasma under pulsed argon ion beam bombardment was investigated. The motion of the particle under the action of the ion beam was observed to be an oscillatory motion. The Fourier-analyzed motion is dominated by the excitation frequency of the pulsed ion beam and odd higher harmonics, which peak near the resonance frequency. The appearance of even harmonics is explained by a variation of the particles's charge depending on its position in the plasma sheath. The Fourier analysis also allows a discussion of neutral and ion forces. The particle's charge was derived and compared with theoretical estimates based on the orbital motion-limited (OML) model using also a numerical simulation of the RF discharge. The derived particle's charge is about 7–15 times larger than predicted by the theoretical models. This difference is attributed to the porous structure of the particle.

[5] Author to whom any correspondence should be addressed.

IOP Institute of Physics ⏀ DEUTSCHE PHYSIKALISCHE GESELLSCHAFT

Contents

1. Introduction

During the last decade, interest in so-called *dusty (complex) plasmas* has increased enormously [1]–[3]. Particles are systematically generated in process plasmas for special applications in materials research, metallurgy, and medicine, or their properties are changed in the plasma [4]. Particles are also used to determine plasma parameters, like electric field strength, energy transport or the density of charge carriers. The background of many of these applications is the specific behavior of powder particles in a radiofrequency (RF) plasma. When particles are inserted into a plasma, they become negatively charged due to the larger mobility of electrons compared to ions. For particles with a diameter of several $10\,\mu$m, this charge can become as large as several $100\,000$ elementary charges [6]. Because of their charge, the particles are sensitive to electric fields. While the gravitational force acting on a sufficiently massive particle tends to pull the particle out of the plasma, the electric field in the plasma sheath above a negatively self-biased RF electrode repels the negatively charged particle and thus acts in the opposite direction. Under certain conditions, i.e. for particles with diameters in the μm regime, the particle encounters a balance between upward (electric) and downward (gravitation) forces and levitates in the sheath region above the electrode. A detailed description of the interaction of these and other forces can be found elsewhere [4, 5], [7]–[9].

So far, particles levitating in a plasma sheath have been manipulated, e.g., with an electric probe [10], with the help of laser beams [11], by time-varying electric fields of an adaptive electrode [12] and by periodic variation of the bias voltage [13]. Once the motion parameters like resonance frequency of the particles or their relative position with respect to the sheath are known, several plasma properties, like sheath thickness and the shape and strength of the electric field in the sheath, and/or particle properties like charge or mass can be determined [14].

In the present experiment, we investigate the interaction of an external ion beam with a particle levitating in an RF plasma sheath. The interaction of an ion compared to a laser beam offers the advantage that at the same beam power a larger momentum can be transferred to the particle [15]. For that purpose, a particle trapped in the sheath was exposed to a pulsed ion beam with known intensity and energy and was thereby excited to an oscillatory motion. A detailed
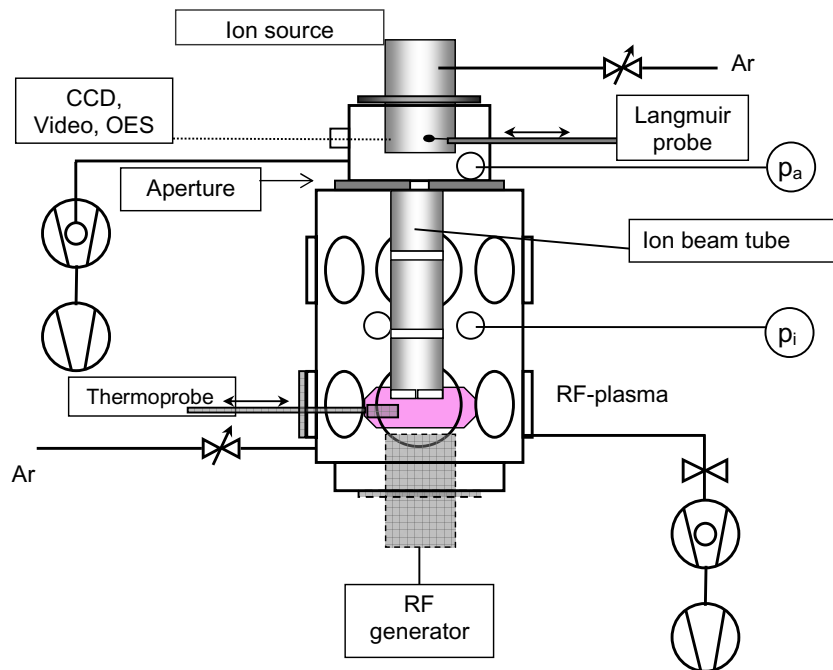
Figure 1. Schematic setup of the PULVA II reactor [15].

analysis of the particle's motion was carried out from which the Fourier frequency spectrum was obtained, which allowed for a discussion of neutral and ion drag forces. The use of a non-spherical porous particle is of interest for a number of applications including technological environments [16], flaking of wall materials in fusion devices [17] and other irregularly shaped objects like spacecraft [18].

2. Experimental setup

The experiments are carried out in the PULVA II reactor [15]. It consists of a cylindrical reactor with a diameter of 400 mm (figure 1) and pumped with the help of a $500 \, 1 \, s^{-1}$ turbomolecular pump to a residual gas pressure of less than 10^{-4} Pa. The effective pumping speed is varied by an adjustable butterfly valve. Argon gas has been admitted by a gas flow controller (MKS) with a flow rate of 30 sccm, yielding a typical operation pressure of 3.5 Pa. An RF discharge is maintained inside the chamber with the help of a planar electrode (diameter 130 mm) located at the bottom of the reactor chamber and driven via a matching network (Dressler VM700) by an RF generator (Dressler Cesar 1310) at 13.56 MHz and with a power of 10 W. Typical plasma parameters are given in table 1.

A vertically expanded laser beam (wavelength 532 nm and power 2 W) is employed for particle illumination. The particle position is recorded through a glass window at 90° with respect to the ion beam and through a narrow filter (530 nm). Two cameras, a reflex camera (Nikon D70) with a focal length of 24–120 mm and a high-speed camera (Nikon FastCam PCI R2) with a frame rate of 125 pictures per second, have been employed. The recorded video sequences are analyzed with a self-written program that calculates the particle's coordinates as a function of time and transfers the particle's positions in chronological order to a spreadsheet.

Table 1. Selected experimental parameters.

Plasma density	$1.5 \times 10^{15}\,\text{m}^{-3}$
Plasma potential	$+15\,\text{V}$
Electron temperature	$3\,\text{eV}$
Self-bias potential	$-300\,\text{V}$
Ion beam energy	$800\,\text{eV}$
Ion beam flux density	$75\,\mu\text{A cm}^{-2}$
Particle diameter	$250\,\mu\text{m}$
Particle mass	$6.9\,\mu\text{g}$
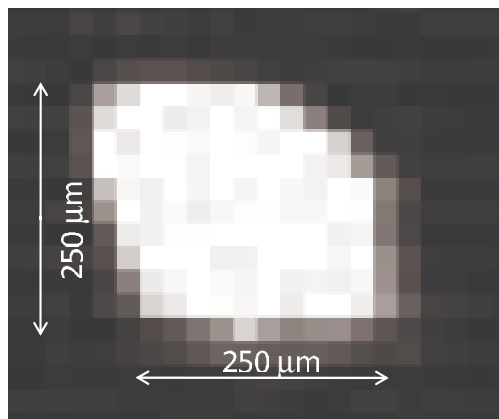
Figure 2. Recorded particle image (1 pixel corresponds to $23\,\mu$m).

Particles are introduced into the plasma with the help of a sieve that is manipulated from the outside. We used SiO_2 powder particles (density $2.2\,\text{g cm}^{-3}$) with a diameter of $0.8\,\mu$m. In addition, the powder contained large agglomerates with sizes of up to about $300\,\mu$m. After several attempts, one lone particle was located in the sheath and its motion was recorded by the camera. The isolated particle displayed in figure 2 was used for the measurements reported below. The particle size of the used agglomerate was estimated at a (mean) diameter of $25\,\mu$m.

In order to estimate the particle's mass m, we performed a series of *ex situ* measurements employing a set of 40 different particles. Particle sizes were measured with a Keyence VHX-100 K digital microscope equipped with a VH-Z100 objective (magnification $\times 100-1000$), employing a digital camera with 2.11×10^6 pixels. The particle mass was measured with a Sartorius SC2 microbalance with a capacity of $2.1\,\text{g}$ and a resolution of $0.1\,\mu$g. Figure 3 displays mass versus mean radius r of the 40 investigated particles. The results closely follow a power law $m = 1.5 \times 10^{-5}\,r^{2.7}$, where m and r are given in μg and μm, respectively. For a mean particle radius of $125\,\mu$m, we get $m = 6.9\,\mu$g, which will be used in the following. It corresponds to a packing density of 38%, which is about half of the maximum close packing density of a face-centered cubic crystal (74%) [19]. The result shows that the particle has a porous structure.

In order to investigate the particle's behavior under the influence of an ion beam, an ion source, EC/A 125 (IOM Leipzig), located at a vacuum port opposite to the RF electrode, is
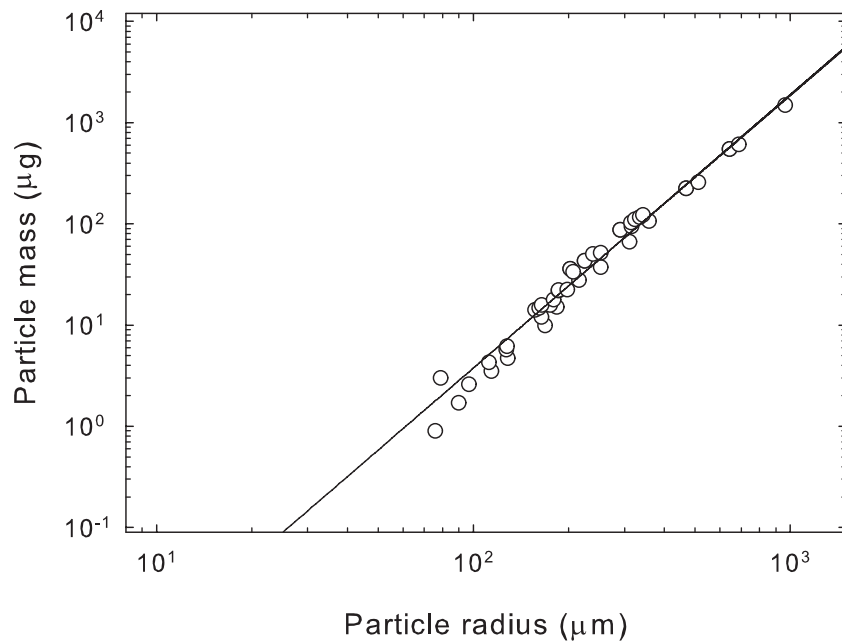
Figure 3. Particle mass m versus mean particle radius r. The solid line corresponds to $m = 1.5 \times 10^{-5}\, r^{2.7}$.

directed downward to the agglomerated particle that is confined in the sheath in front of the RF electrode. The ion beam is guided by a stainless steel tube with an inner diameter of 7.5 cm and leaving the tube through a grounded plate with a center orifice of 0.5 cm (see figure 1). The ion source is operated with a gas flow of 8 sccm argon at a pressure of 0.06 Pa, maintained by a separate turbo pump (Leybold) with a pumping speed of $1500\,1\,s^{-1}$. For pulsed operation, the ion source is driven with a square wave voltage in the frequency range 0.1–8 Hz and with a duty cycle of 1:1.

3. RF plasma simulation

We have performed a numerical simulation of the RF discharge in order to model the discharge characteristics. A one-dimensional (1D) model of the RF discharge is used, which is expected to provide rather realistic plasma parameters of the RF plasma sheath as long as the dust particle is placed close to the central axial discharge region and still is computationally treatable on a single CPU on a standard PC. By using the experimentally known time-dependent bias voltages, the model represents quite well the dynamics of the potential, densities and velocities of all species [20, 21]. The simulation yields discharge parameters such as temperature, plasma potential, velocity and density of plasma species (Ar^+, e^-) at various positions in the discharge including the dust particle location. The computational tool uses a particle-in-cell with Monte Carlo collisions (PIC-MCC) code and allows for a kinetic treatment of all plasma particles [22]–[25]. The kinetics of 'super particles' representing many real particles moving in self-consistent fields discretized on a grid are followed. The collisions between particles are modeled using a binary Coulomb collision model described in [23, 25], and MCC models are used for other types of collisions. The PIC code allows us to self-consistently resolve the whole plasma including the electrostatic sheath in front of the material wall.
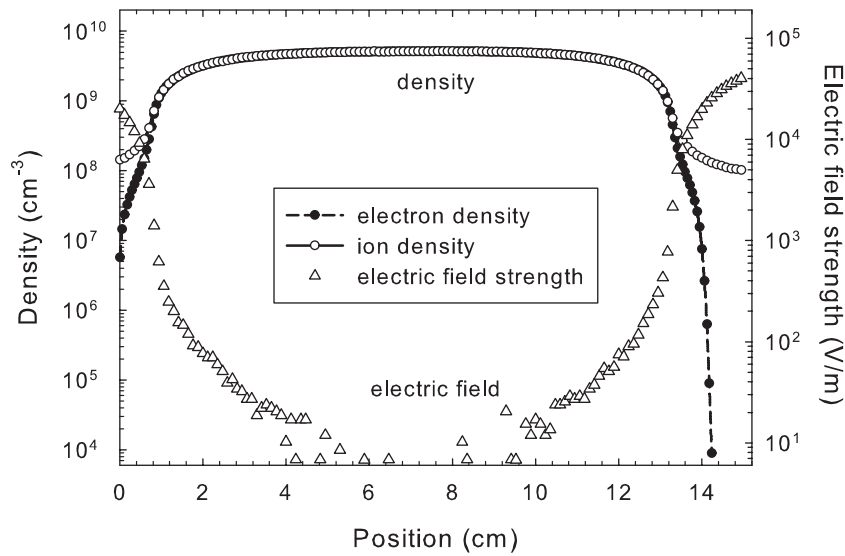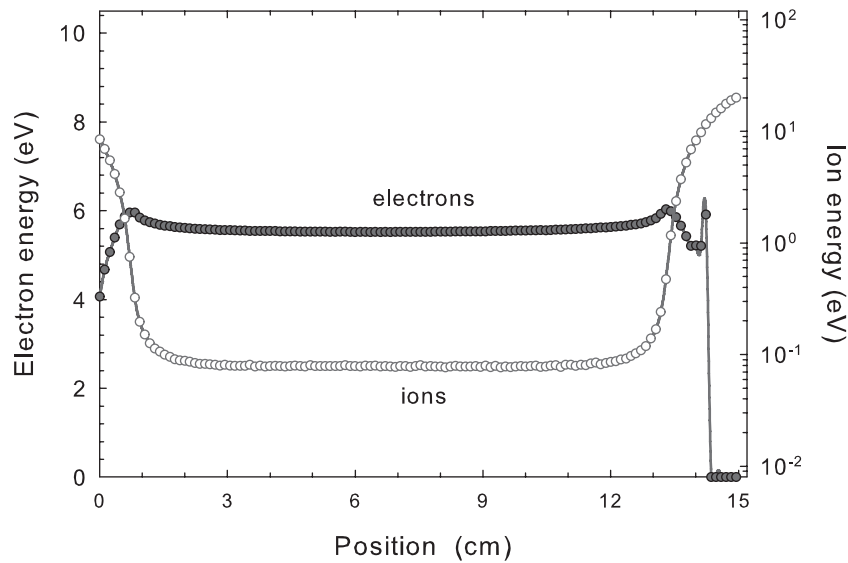
Figure 4. Simulated electron (●) and ion (○) density versus position. The figure also shows the outward directed electric field strength $|E|$. Note that the electric field strength $\vec{E}$ crosses zero and changes sign near the plasma center.

The parameters of the simulation were chosen to reasonably resemble the essential features of the experiment. In the simulation, a parallel plate reactor with a separation of 15 cm between the electrodes was employed. The powered electrode was placed at a position $z = 15$ cm with the grounded electrode at $z = 0$ cm. The RF voltage applied to the powered electrode is given by $U_{RF} = U_{bias} + U_0 \sin(\omega t)$, where $U_{bias} = -300$ V and $U_0 \approx 315$ V. This means that the simulations take into account the asymmetric behavior of the discharge. The collisions included for the current study are Coulomb, elastic and inelastic collisions between the various plasma species [24].

The calculated discharge characteristics are typical for a collisionless RF discharge. Figures 4 and 5 display the calculated (electron and ion) densities and the corresponding energies, respectively, in the axial direction between the electrodes. Obviously, electron and ion densities are equal in the discharge center but strongly deviate in the sheath regions near the electrodes.

The simulated time-averaged plasma potential and the derived electric field strength are displayed in figure 6. The plasma potential is zero at the grounded electrode (at $z = 0$ cm) and drops to -300 V at the powered electrode (at $z = 15$ cm); it attains a large positive value of $\approx +90$ V in the plasma center. The latter value deviates from the experimental plasma potential of $+15$ V.

The computed sheath width at the powered and the grounded electrode is 1.8 and 0.8 cm, respectively. The simulated electric field strength as derived from the variation of the plasma potential is also shown in figure 6. It yields an outward (towards the electrodes) directed electric field $\vec{E}$ which is zero near the plasma center, where it changes sign. The electric field in the sheath region accelerates ions towards the electrodes while electrons are repelled. This is reflected in the energy distribution of both ions (which become supersonic in the sheath) and electrons (figure 5).

Figure 5. Simulated electron (●) and ion (○) energy versus position.
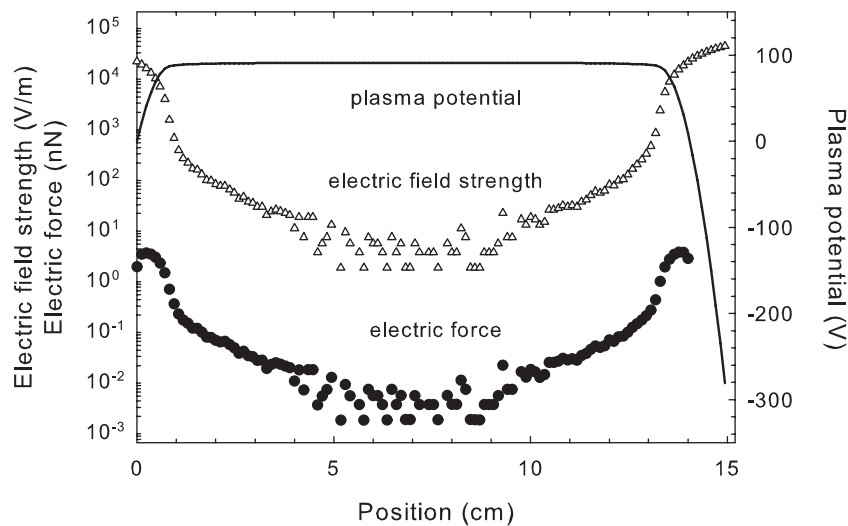
Figure 6. Simulated plasma potential (solid line), electric field strength (△) and electric force acting on the particle (●) versus position.

4. Results and discussion

The particle motion under the influence of a square wave-modulated ion beam with a beam energy of 800 eV and a modulation frequency of 0.5 Hz is displayed in figure 7. By interaction with the ion beam (*on* period), the trapped particles are displaced from their original position and start to oscillate around a new equilibrium position. During the ion beam *off* period, the particle resumes to its initial equilibrium position where it continues to oscillate. At this low excitation frequency, the particle oscillates with a frequency close to its eigen or resonance frequency superimposed on the modulation frequency of the ion beam.
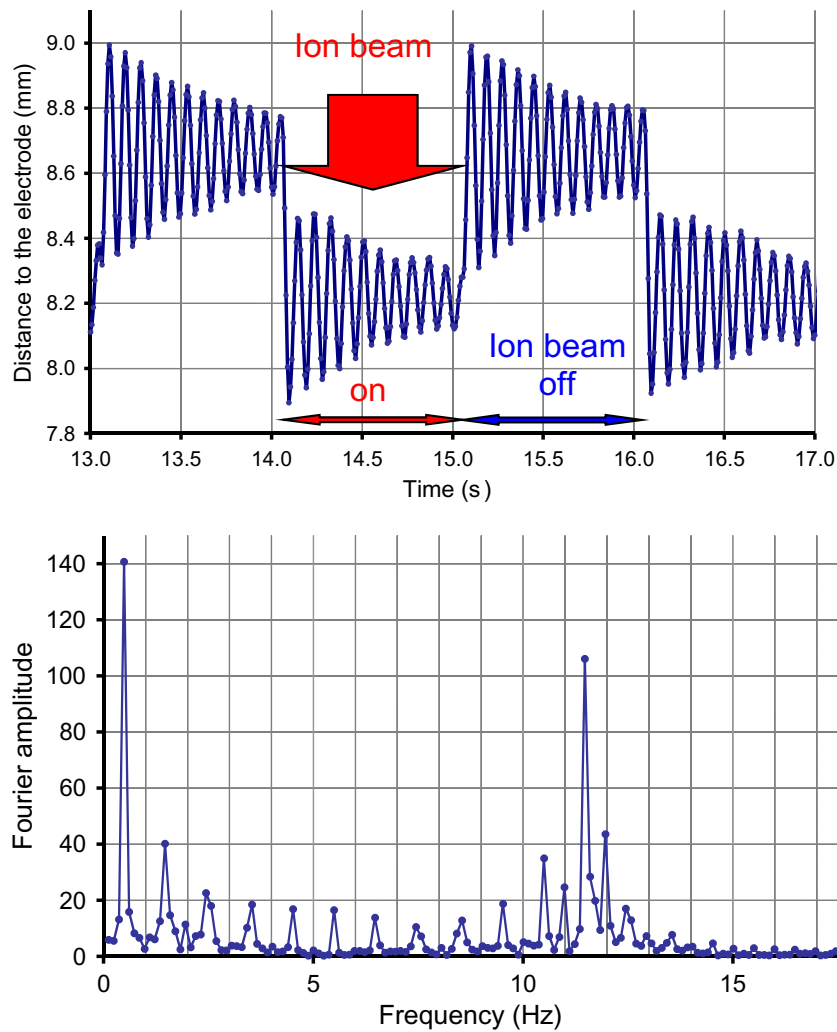
Figure 7. Top: particle position following ion beam excitation at 0.5 Hz. Bottom: experimental Fourier coefficients derived from the particle's movement.

The chronological course of the particle's movement was evaluated and a Fourier analysis was carried out in order to determine the particle's frequency spectrum. The deduced frequency spectrum (figure 7) shows two major components: the excitation frequency ($\nu_a = 0.5$ Hz) of the ion beam and an enhancement in the Fourier spectrum at the resonance frequency $\nu_r \approx 11.3$ Hz of the particle in the plasma. The Fourier spectrum also contains odd higher harmonics, while even harmonics, except in the neighborhood of the resonance frequency, are suppressed. For the particle oscillation, the back driving force is the difference between the field force, generated by the electric field in the sheath, and the gravitation force on the particle. Since the electric field has an almost linear dependence with distance, the particle's motion resembles that of a linear oscillator. The approximate linearity of the electric field, based on the parabolic shape of the potential, has been asserted, e.g., by Tomme *et al*, who carried out investigations with oscillating particles and showed that over a distance of 20% of the sheath thickness, the divergence from a parabolic potential is small [26].

In the following, we assume that the particle is trapped in the plasma sheath at an equilibrium position z_{eq} above the RF electrode, where the electrostatic force $F_e = QE$ due to the electric field E in the plasma sheath is balanced by the gravitational force $F_g = mg$ acting on the particle's mass m, i.e. $F_e(z_{eq}) = F_g$, where $g = 9.81\,\text{m s}^{-2}$ is the gravitational acceleration, Q is the electric charge on the particle and $E = E(z)$ is the electric field strength. Furthermore, we assume that the restoring force $F_R = F_e - F_g$ in the neighborhood of z_{eq} varies linearly with particle height z above the electrode, i.e.

$$F_R = -\kappa(z - z_{eq}). \tag{1}$$

Following Tomme *et al* [26], we then express the equation of motion as

$$m\ddot{z} + 2\gamma\dot{z} + \kappa(z - z_{eq}) = F(t), \tag{2}$$

where 2γ is the damping constant, κ the restoring constant and $F(t)$ an external force acting on the particle. For the simple damped harmonic oscillator (equation (2) with $F = 0$), we obtain [26]

$$\kappa = m\omega_r^2 + \frac{\gamma^2}{m} \approx m\omega_r^2 \tag{3}$$

with ν_r being the eigenfrequency, and $\omega_r = 2\pi\nu_r$ and $m\omega_r^2 \gg \gamma^2/m$ are the conditions considered here.

4.1. Particle's charge

The accumulated negative charge at the particle can be estimated from its equilibrium position $z_{eq} = 0.87\,\text{cm}$ with the ion beam *off*. We assume a linear variation of the electric force with particle height z above the electrode, i.e.

$$E(z) = 2\frac{\Delta V}{d_s}\left(1 - \frac{z}{d_s}\right), \tag{4}$$

with $\Delta V = V_{bias} - V_{pl}$. Here, d_s is the position of the sheath edge, $V_{bias} = -300\,\text{V}$ is the electrode self-bias potential and $V_{pl} = 15\,\text{V}$ is the plasma potential. The position of the sheath edge is estimated from the position of the smaller (diameter of $0.8\,\mu\text{m}$) and thus considerably lighter particles that are trapped at $z = 1.05\,\text{cm}$; this position approximately corresponds to the sheath edge. Using $F_e(z_{eq}) = QE(z_{eq}) = F_g$, we obtain $Q = -4.1 \times 10^7$ elementary charges.

Likewise, we can calculate the particle's charge from the restoring constant $\kappa \approx m\omega_r^2 = 3.5 \times 10^{-5}\,\text{kg s}^{-2}$ (equation (3)), which we obtain with the deduced resonance frequency $\nu_r = 11.3\,\text{Hz}$ and a particle mass $m = 6.9\,\mu\text{g}$. Expressing the restoring constant κ as the gradient of the restoring force,

$$\kappa = \frac{\partial F}{\partial z} = Q\frac{\partial E}{\partial z} + E\frac{\partial Q}{\partial z}, \tag{5}$$

we obtain, for a constant Q and with $\partial E/\partial z = -5.7 \times 10^6\,\text{V m}^{-2}$ (equation (4)), $Q = -3.8 \times 10^7$ elementary charges, in fair agreement with the previous estimate.

For a theoretical estimate of the particle's charge, we consider the ion and electron currents flowing to the particle. For the electron current density j_e and the ion current density j_i, we use the orbital motion-limited (OML) currents [27]

$$j_e = e_0 n_e \sqrt{\frac{kT_e}{2\pi m_e}}\exp\left(\frac{e_0\phi}{kT_e}\right), \tag{6}$$

and

$$j_{\mathrm{i}} = e_0 n_{\mathrm{i}} \sqrt{\frac{kT_{\mathrm{i}}}{2\pi m_{\mathrm{i}}}} \left(1 - \frac{e_0 \phi}{kT_{\mathrm{i}}}\right), \tag{7}$$

where the surface potential ϕ of the particle is connected to the particle's charge Q via

$$Q = 4\pi \epsilon_0 r \left(1 + \frac{r}{\lambda_{\mathrm{d}}}\right) \phi, \tag{8}$$

and where

$$\lambda_{\mathrm{d}} = \sqrt{\frac{\epsilon_0 k}{e_0^2 (n_{\mathrm{e}}/T_{\mathrm{e}} + n_{\mathrm{i}}/T_{\mathrm{i}})}} \tag{9}$$

is the Debye screening length. T_{e} and T_{i} are electron and ion temperatures, m_{e} and m_{i} are electron and ion masses, e_0 is the elementary charge and k is the Boltzmann constant. Likewise, since the particle resides outside the plasma in the sheath region, we may use the Bohm ion flux

$$j_{\mathrm{i}} = 0.6 e_0 n_{\mathrm{i}} \sqrt{\frac{kT_{\mathrm{e}}}{m_{\mathrm{i}}}} \tag{10}$$

instead of equation (7).

Under equilibrium conditions, the sum of the electron and ion currents to the particle disappears. Further assuming quasi-neutrality ($n_{\mathrm{e}} = n_{\mathrm{i}}$) and combining equations (10) and (6), we obtain

$$\phi = \frac{kT_{\mathrm{e}}}{2e_0} \ln\left(\frac{0.72\pi m_{\mathrm{e}}}{m_{\mathrm{i}}}\right). \tag{11}$$

On the basis of the Bohm ion flux (equation (10)) and using $T_{\mathrm{e}} = 3\,\mathrm{eV}$ and $n_{\mathrm{e}} = 1.5 \times 10^{15}\,\mathrm{m}^{-3}$ [28], we obtain $\phi = -15.6\,\mathrm{V}$ and $Q = -6.1 \times 10^6$ elementary charges. This value is almost 7 times smaller than the measured charge on the particle. An even smaller value of $Q = -2.9 \times 10^6 e_0$ is obtained when using the OML (equation (7)) rather than the Bohm (equation (10)) ion flux. Kindly note that a non-Maxwellian electron energy distribution function displaying a high-energy tail should not influence these results significantly. As is obvious from equation (11), the particle's charge depends linearly on the electron temperature T_{e} and thus a drastic temperature variation would be required to explain the measured charge.

We also mention the alternative approach of Bronold *et al* [29] that is based on a balance between inflowing and outflowing electrons. Accordingly, the particle's charge is given by

$$Q = 4\pi r^2 \frac{e_0 h}{kT_{\mathrm{p}}} \exp\left(\frac{W_{\mathrm{e}}}{kT_{\mathrm{p}}}\right) j_{\mathrm{e}}, \tag{12}$$

where h is Planck's constant, T_{p} the particle temperature and j_{e} the OML electron flux (equation (6)) to the particle, while the ion flux to the particle is neglected. The electron binding energy W_{e} is expressed as

$$W_{\mathrm{e}} = \frac{R}{16} \frac{(\epsilon - 1)^2}{(\epsilon + 1)^2}, \tag{13}$$

where R is the Rydberg energy and ϵ is the relative dielectric constant of the particle ($\epsilon \approx 4.5$ for SiO_2 [30]). This yields an electron binding energy $W_{\mathrm{e}} = 0.344\,\mathrm{eV}$, much smaller than the photon energy of the illuminating laser ($2.34\,\mathrm{eV}$). Thus, a significant electron detachment by the
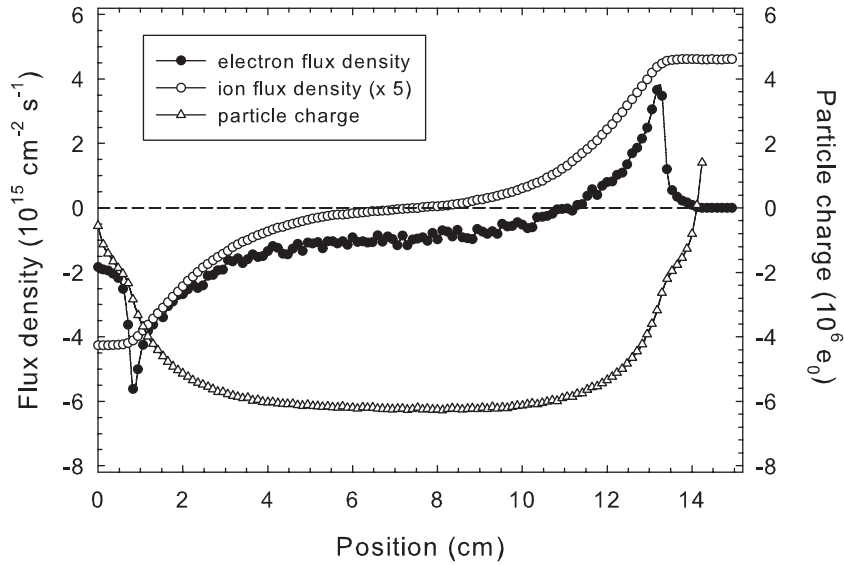
Figure 8. Simulated electron (●) and ion (○) flux density versus position. The resulting particle charge (△) is also shown.

laser light should occur. This should reduce the particle's charge, which has not been observed, however. Even without this additional complication, the model is insufficient to explain the measured charge on the particle.

The electron and ion fluxes from the PIC simulation of the RF plasma and the resulting charge on the particle are shown in figure 8. The plasma parameters together with analytical models like OML or the Khrapak model are used to compute the dust charge in the RF discharge [27, 31]. The predicted charge at the particle if placed inside the plasma bulk amounts to about -6.3×10^6 elementary charges, which is in reasonable agreement with the charge obtained from the analytical analysis (see above).

The inward (into the plasma) directed electric force $|Q\vec{E}|$ acting on the particle is displayed in figure 6. The force shows pronounced maxima in the sheath regions in front of the grounded and powered electrodes at positions $z \approx 0.23$ and 13.8 cm, respectively. The latter value is close to the actual particle position at $z \approx 14.1$ cm. The calculated electric field force is insufficient to compensate for the gravitation force, which exceeds the electric field force by more than one order of magnitude.

Thus, the simulation does not improve the analytical results, and other reasons for the apparent discrepancy have to be sought. One possible reason is the porous structure of the particle. A simple estimate shows that the particle's inner surface is about two orders of magnitude larger than its outer surface, and this could give rise to a much larger charge than calculated with the spherical condenser model (equation (8)).

Other possible reasons are (i) the non-spherical shape, (ii) the non-conducting (insulating) material and (iii) the size of the particle which affects the electrostatic force acting on it. According to Daugherty *et al* [32], we have to replace the electric field strength E by an effective field E_{eff} and the electrostatic force F_e by

$$F_e = Q \left[E \left(1 + \frac{(r/\lambda_d)^2}{3(1 + r/\lambda_d)} \right) \right]. \tag{14}$$

An estimation shows that under the conditions considered here this effect accounts for a factor of 1.2, which is again insufficient to explain the deviation.

Upper limits for the particle charge have been discussed, e.g., by Trottenberg *et al* [33]. Accordingly, the electric charge on a particle is limited by electron field emission and by field-induced evaporation. The electric field strength E_p on the surface of a spherical particle with radius r is related to its specific charge Q/m:

$$E_p = \frac{r\rho}{3\epsilon}\frac{Q}{m} \tag{15}$$

with ρ being the particle density. Taking $Q = 4 \times 10^7$ elementary charges and $m = 6.9\,\mu g$, we obtain $E_p \approx 10^7\,\mathrm{V\,m^{-1}}$. The value is significantly lower than the limits set by electron field emission ($|E_p| > 10^9\,\mathrm{V\,m^{-1}}$) and by field desorption ($|E_p| > 10^{10}\,\mathrm{V\,m^{-1}}$).

4.2. Neutral drag force

The decay constant

$$\tau = m/\gamma \tag{16}$$

is related to the neutral drag and, hence, the viscosity η the particle experiences in the surrounding gas. Making use of Stokes' law [34], we express the damping constant γ by the viscosity η as

$$\gamma = 3\pi\eta r, \tag{17}$$

from which we obtain $\eta = 5.8\,\mu\mathrm{Pa\,s}$ for $\tau = 1\,\mathrm{s}$ (see figure 7). This value is significantly lower than the standard value for argon of $\eta = 22.4\,\mu\mathrm{Pa\,s}$ [35]. It is well known, however, that equation (17) does not hold for small particle sizes of the order of the mean free path λ. Applying Cunningham's correction [36, 37], we obtain an effective viscosity

$$\eta_{\mathrm{eff}} = \eta\frac{r}{r + A\lambda}, \tag{18}$$

where r is the particle radius,

$$A = \alpha + \beta\exp(-\xi r/\lambda), \tag{19}$$

and with the parameters $\alpha = 1.227$, $\beta = 0.42$ and $\xi = 0.85$ taken from [35]. The calculated correction is rather large and yields $\eta_{\mathrm{eff}} = 0.89\,\mu\mathrm{Pa\,s}$ at a pressure of 3.5 Pa. A similar value of $0.85\,\mu\mathrm{Pa\,s}$ is obtained making use of Epstein's expression [38, 39]. Both values are significantly smaller than the experimental value of $5.8\,\mu\mathrm{Pa\,s}$ (see above). However, considering a likely roughness of the particle's surface and its porosity, the difference does not appear unrealistic.

4.3. Ion drag force

For sufficiently high energies and a sufficiently large particle, the ion drag force exerted by the external ion beam may be calculated from the momentum transfer $m_b v_b$ multiplied by the ion flux density $n_b v_b$ and the particle's cross-sectional area,

$$F_i = \pi r^2 n_b m_b v_b^2, \tag{20}$$

where n_b is the ion beam density, v_b the ion velocity and m_b the ion mass. The ion velocity is calculated from the ion energy as extracted from the ion source by the source potential U_s:

$$v_b = \sqrt{\frac{2e_0 U_s}{m_b}}, \tag{21}$$

whereas the ion density was obtained from the energy influx of $0.06\,\text{J cm}^{-2}\,\text{s}^{-1}$ measured by a thermal probe [15, 40]. For an ion beam energy $e_0 U_s = 800\,\text{eV}$, we thus obtain $F_i = 9.5 \times 10^{-10}\,\text{N}$. We can compare this number with the force $\Delta F = \kappa \overline{\Delta z} = 1.6 \times 10^{-8}\,\text{N}$ required for a mean particle displacement of $\overline{\Delta z} = 4.5 \times 10^{-4}\,\text{m}$ during its interaction with the ion beam (figure 7). Comparing the two forces we note that the estimated ion drag force, only accounts for 6% of the calculated ΔF.

4.4. Particle de-charging

The difference between the two forces is attributed to the particle's de-charging by the action of the ion beam. In order to estimate the de-charging effect, we again consider the ion (equation (7) or (10)) and electron (equation (6)) currents to the particle to which we add the contribution from the ion beam

$$j_i^{\text{beam}} = e_0 n_b v_b (1 + \delta) \tag{22}$$

and where secondary electron emission by the impact of energetic ions is accounted for by the $1 + \delta$ term, with δ being the secondary electron emission coefficient for energetic ion impact. Typically, $\delta \approx 0.1$ for secondary emission of electrons bound to solids [41] and as such it is not expected to provide a significant additional contribution.

Under equilibrium conditions the total current to the particle disappears. Assuming quasi-neutrality ($n_e = n_i$) and combining equations (10) and (22) with equation (6), we obtain

$$\exp\left(\frac{e\phi}{kT_e}\right) = \frac{0.6 n_i \sqrt{kT_e/m_i} + n_b v_b (1 + \delta)}{n_e \sqrt{kT_e/2\pi m_e}} \tag{23}$$

and, hence,

$$\Delta\phi = \frac{kT_e}{e_0} \ln\left(1 + \frac{n_b v_b (1 + \delta)}{0.6 n_i \sqrt{kT_e/m_i}}\right), \tag{24}$$

where $\Delta\phi \equiv \phi - \phi_0$, ϕ_0 is the surface potential without ion beam ($n_b = 0$) and

$$\frac{\Delta Q}{Q} = \frac{\Delta\phi}{\phi_0} = 2 \frac{\ln\left(1 + \frac{n_b v_b (1 + \delta)}{2.4 n_i \sqrt{kT_e/m_i}}\right)}{\ln\left(0.72\pi \frac{m_e}{m_i}\right)} \tag{25}$$

in connection with equation (8). Furthermore, making use of

$$\frac{\partial F}{\partial z} = Q \frac{\partial E}{\partial z} + E \frac{\partial Q}{\partial z},$$

we obtain

$$\frac{\Delta Q}{Q} = \frac{\Delta F}{F} - \frac{\Delta E}{E} \approx 0.94 \times \frac{\Delta F}{F},$$

as we attribute 6% of ΔF to the ion drag force and the remaining 94% to the particle's de-charging by the ion beam (see section 4.3). With $\Delta F = 1.6 \times 10^{-8}$ N and $F = F_g = 6.8 \times 10^{-8}$ N, we obtain $\Delta Q/Q \approx 22.1\%$.

From our theoretical analysis based on the Bohm ion flux (equation (25)) using $T_e = 3$ eV and $n_e = 1.5 \times 10^{15}$ m^{-3} [28], we obtain $\Delta Q/Q \approx 16.4\%$, which is in fair agreement with experiment. The value of $\Delta Q/Q \approx 3.0\%$ is much smaller, which we obtain if we use the OML (equation (7)) rather than the Bohm (equation (10)) ion flux. One explanation for this discrepancy may be due to an overestimation of the ion current in the sheath region as predicted by the OML model. As ions become considerably accelerated when leaving the plasma, their energy in the plasma sheath drastically differs from their initial energy within the plasma. This has the consequence that the $1 - e_0\phi/kT_i$ term in equation (7), which accounts for an enhanced ion collection by the particle, becomes too large if the initial (thermal) T_i is used. A modification of this term making use of, e.g., $T_i = T_e/2$ as follows from the Bohm theory [42] will thus lead to a significantly larger value of $\Delta Q/Q \approx 9.0\%$ compared with the previous value.

4.5. Fourier frequency spectrum

For the square wave-modulated ion beam that we used for interaction with the particle, we can express the external force $F(t)$ as a Fourier series,

$$F(t) = \frac{F_0}{2}\left(1 - \frac{4}{\pi}\sum_{n=1}^{m} f_n \sin(\omega_n t)\right), \tag{26}$$

where $\omega_n = 2\pi(2n-1)\nu_a$, with ν_a being the square wave modulation (excitation) frequency of the ion beam, and where the Fourier coefficients f_n are given by

$$f_n = \frac{1}{2n-1}. \tag{27}$$

The solution of $z(t)$ is obtained as

$$z(t) = \frac{F_0}{m}\left(\frac{1}{2\omega_r^2} + \frac{2}{\pi}\sum_{n=1}^{m} a_n f_n \sin(\omega_n t - \varphi_n)\right), \tag{28}$$

where

$$a_n = \frac{1}{\sqrt{(\omega_r^2 - \omega_n^2)^2 + (2\gamma\omega_n)^2}}, \tag{29}$$

$$\varphi_n = \arctan\left(\frac{2\gamma\omega_n}{m(\omega_r^2 - \omega_n^2)}\right), \tag{30}$$

and $0 \leqslant \varphi_n \leqslant \pi$.

As a consequence, the theoretical frequency spectrum only contains odd harmonics. The experimental results for $\nu_a = 0.5$ Hz rather well follow this prediction (figure 9). Deviations appear in the vicinity of the resonance frequency where even side bands develop. The origin of these may be traced back to the before-mentioned de-charging due to the incident ion beam.

A closer inspection of figure 7 reveals significantly different oscillation frequencies for the cases with ion beam *off* and *on*. Figure 10 shows a separate Fourier analysis of the experimental
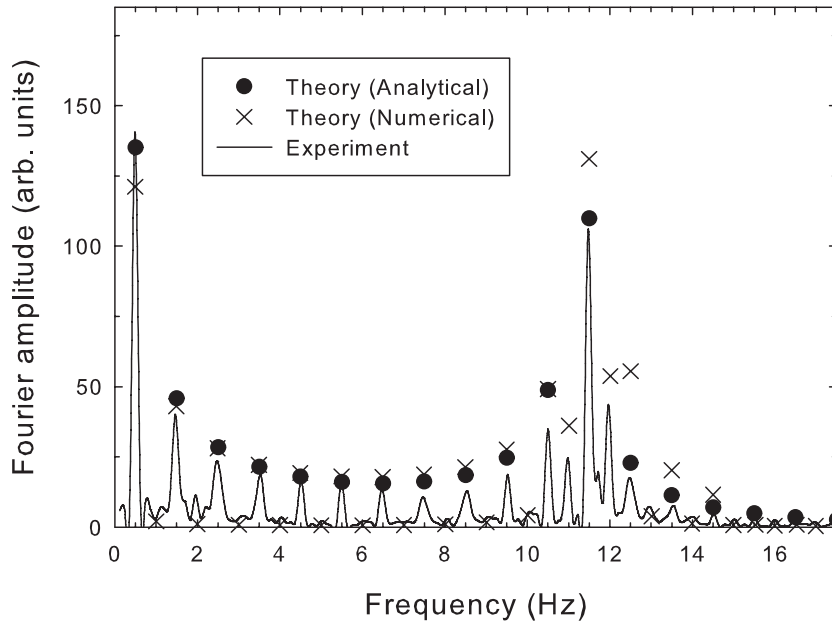
Figure 9. Comparison of experimental and theoretical Fourier coefficients following ion beam excitation at 0.5 Hz.
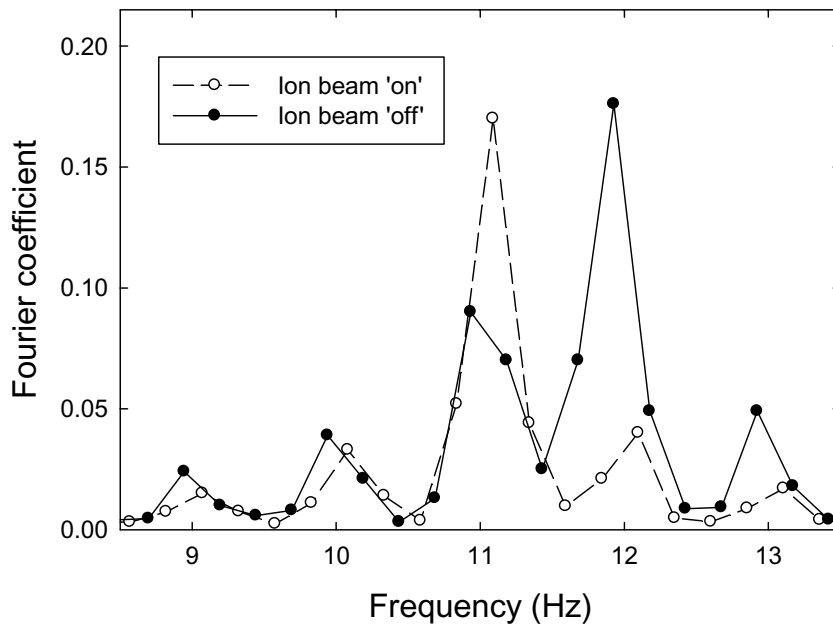
Figure 10. Separate Fourier analysis for the cases at ion beam *on* and *off* following ion beam excitation with 0.5 Hz.

data for the two cases with ion beam *off* and *on*. Apparently, the two cases have slightly different resonance frequencies, which can be explained by a different restoring force due to differing particle charges at the two positions. The relative frequency difference $\Delta \nu_r / \nu_r$ amounts to about 7%; as the restoring force and, hence, the particle's charge depend quadratically on the resonance frequency, this corresponds to a relative charge difference $\Delta Q / Q \approx 2 \times 7\% = 14\%$,
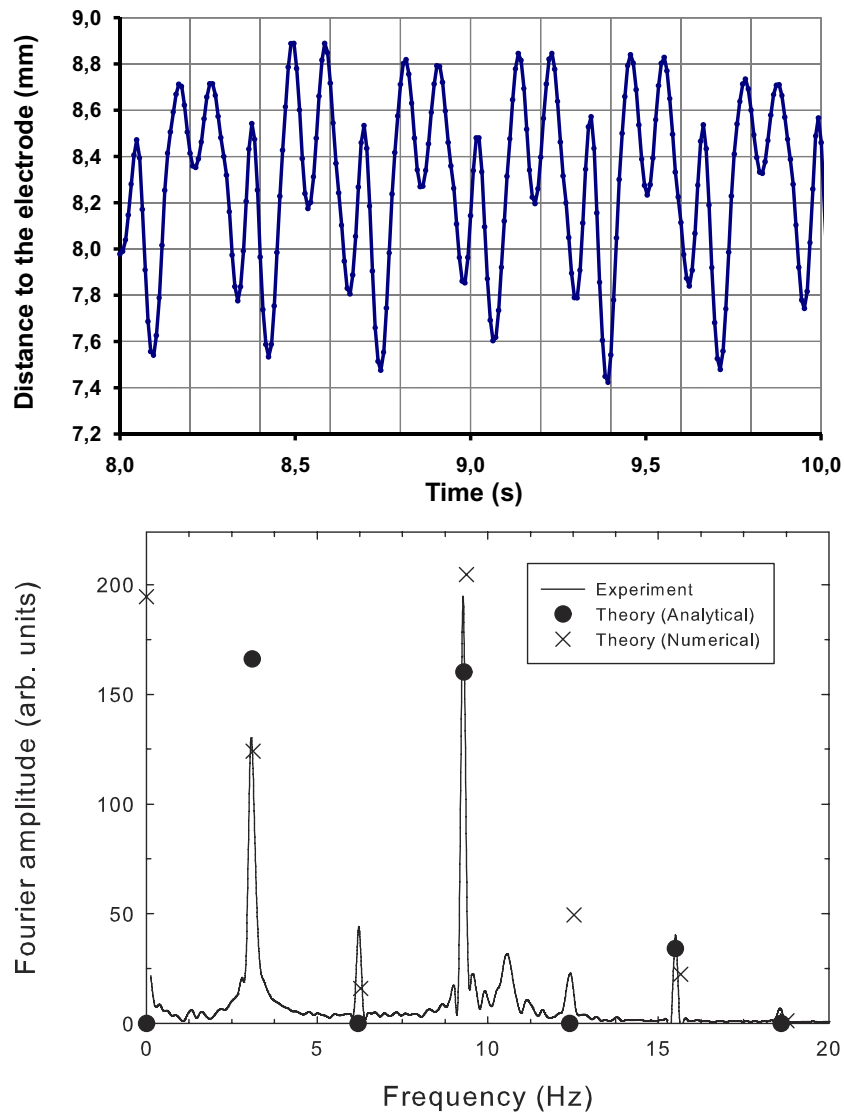
Figure 11. Particle position following ion beam excitation at 3.1 Hz (top) and the corresponding frequency spectrum obtained by Fourier analysis (bottom).

i.e. about twice the frequency difference. The result thus provides further confirmation of the particle's de-charging as derived in section 4.4.

The particle's de-charging in the plasma sheath leads to a deviation from a harmonic potential and to a restoring force F_R that is no longer linearly depending on the particle's position z (equation (1)). Rather, we approximate F_R by

$$F_R = \kappa (z - z_{eq}) \times \left(1 + 2 \frac{\Delta \omega_r}{\omega_r} \frac{(z - z_{eq})}{\overline{\Delta z}} \right) \tag{31}$$

and we arrive at the numerical solutions shown in figure 9, which reproduces the experimental finding.

At an excitation frequency $\nu_a = 3.1\,\text{Hz}$, the particle motion is largely governed by a combination of the fundamental frequency and the third harmonic at 9.3 Hz (figure 11).
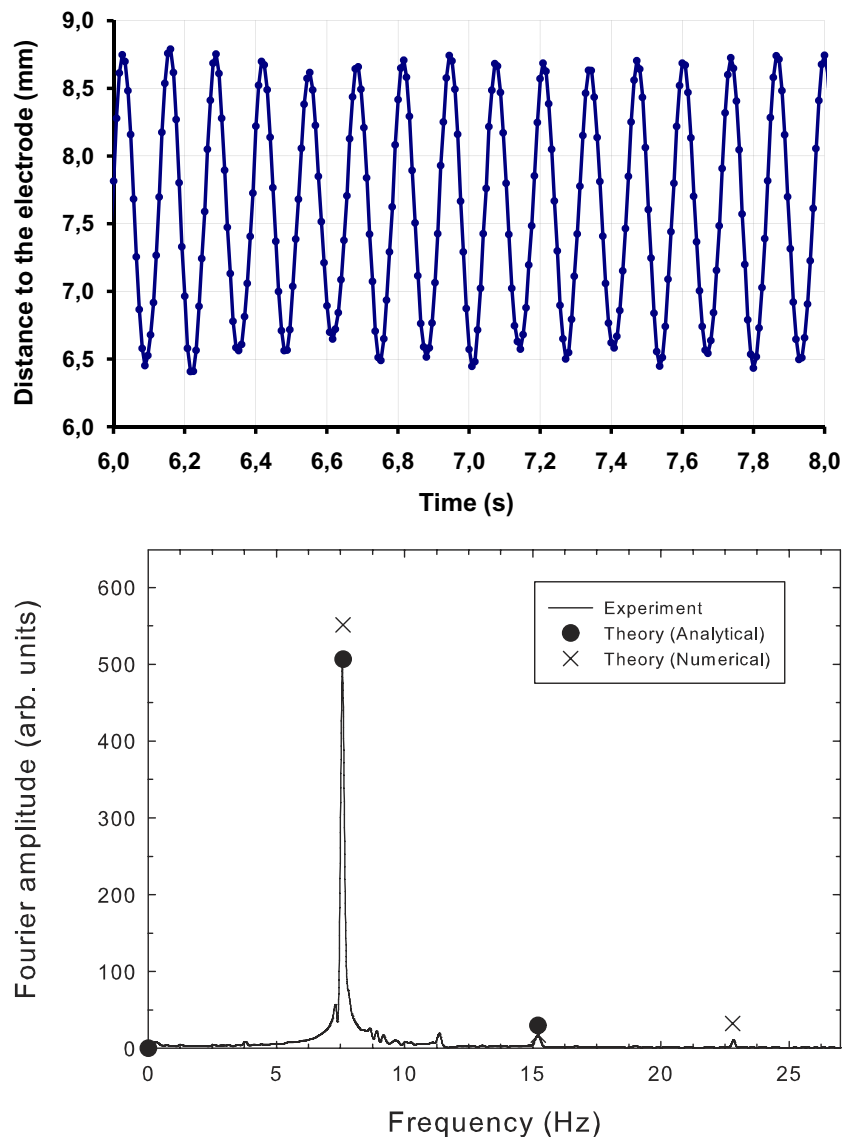
Figure 12. Particle position following ion beam excitation at 7.6 Hz (top) and corresponding frequency spectrum obtained by Fourier analysis (bottom).

However, other frequencies corresponding to the even second and fourth harmonics also occur. The result is in fair agreement with the theoretical analysis.

At an excitation frequency $\nu_a = 7.6$ Hz, the particle motion is dominated by the first harmonic (figure 12). The particle motion almost fully follows the excitation frequency and higher harmonics do not play a significant role. The experimental results are in excellent agreement with the theoretical prediction.

5. Conclusion

The accumulated charge of about 4×10^7 elementary charges on a levitating porous particle with a diameter of $250\,\mu$m in an RF plasma was found to be about one order of magnitude

larger than predicted by theoretical models. The difference is attributed to the porous structure of the particle. This is experimentally supported by the scaling of the particle mass versus mean particle radius. The particle motion under the action of the pulsed ion beam displays an oscillatory motion. The Fourier-analyzed motion is dominated by the excitation frequency and odd higher harmonics that peak near the resonance frequency. The appearance of even harmonics is explained by a variation of the particle's charge depending on its position in the plasma sheath. Furthermore, the results of this study demonstrate that particle oscillations due to the action of an external ion beam can be used for the probing of complex plasma environments.

Acknowledgments

References

[1] Vladimirov S V, Ostrikov K and Samarian A A 2005 *Physics and Applications of Complex Plasmas* (London: Imperial College Press)
[2] Mendonça J T, Resendes D P and Shukla P K (ed) 2008 *Multifacets of Dusty Plasmas* (*AIP Conf. Proc.* vol 1041)
[3] Shukla P K and Eliasson B 2009 *Rev. Mod. Phys.* **81** 25
[4] Hippler R and Kersten H 2008 Applications of dusty plasmas *Low Temperature Plasmas* vol 2 ed R Hippler, H Kersten, M Schmidt and K H Schoenbach (Berlin: Wiley) pp 787
[5] Barnes M S, Keller J H, Forster J C, O'Neill J.A and Coultas D K 1992 *Phys. Rev. Lett.* **68** 313
[6] Tomme E B, Law D A, Annaratone B M and Allen J E 2000 *Phys. Rev. Lett.* **85** 2518
[7] Melzer A and Goree J 2008 Fundamentals of dusty plasmas *Low Temperature Plasmas* vol 1 ed R Hippler, H Kersten, M Schmidt and K H Schoenbach (New York: Wiley) pp 129
[8] Bouchoule A (ed) 1999 *Dusty Plasmas* (New York: Wiley) pp 27ff
[9] Piel A, Arp O, Block D, Pilch I, Trottenberg T, Käding S, Melzer A, Baumgartner H, Henning C and Bonitz M 2008 *Plasma Phys. Control. Fusion* **50** 124003
[10] Konopka U, Morfill G E and Ratke L 2000 *Phys. Rev. Lett.* **84** 891
[11] Melzer A 2001 *Phys. Scr.* T **89** 33
[12] Basner R, Sigeneger F, Loffhagen D, Schubert G, Fehske H and Kersten H 2009 *New J. Phys.* **11** 013041
[13] Kortshagen U and Mümken G 1996 *Phys. Lett.* A **217** 126
[14] Samarian A A and James B W 2005 *Plasma Phys. Control. Fusion* **47** B629
[15] Kersten H, Wiese R, Neumann H and Hippler R 2006 *Plasma Phys. Control. Fusion* **48** B105
[16] Garscadden A, Ganguly B N, Haaland P D and Williams J 1994 *Plasma Sources Sci. Technol.* **3** 239
[17] Winter J 1998 *Plasma Phys. Control. Fusion* **40** 1201
[18] Whipple E C 1981 *Rep. Prog. Phys.* **44** 1197
[19] Kittel C 1995 *Introduction to Solid State Physics* 7th edn (New York: Wiley)
[20] Bronold F X, Matyash K, Tskhakaya D, Schneider R and Fehske H 2007 *J. Phys. D: Appl. Phys.* **40** 6583–92
[21] Matyash K, Schneider R, Dittmann K, Meichsner J, Bronold F X and Tskhakaya D 2007 *J. Phys. D: Appl. Phys.* **40** 6601–7
[22] Matyash K and Schneider R 2006 *J. Plasma Phys.* **72** 809
[23] Matyash K, Schneider R, Tacogna F, Hatayama A, Longo S, Capitelli M, Tskhahaya D and Bronold F X 2007 *Contrib. Plasma Phys.* **47** 595

[24] Ikkurthi V R, Matyash K, Melzer A and Schneider R 2008 *Phys. Plasmas* **15** 123704

[25] Takizuka T and Abe H 1977 *J. Comput. Phys.* **25** 205–19

[26] Tomme E B, Annaratone B M and Allen J E 2000 *Plasma Sources Sci. Technol.* **9** 87

[27] Allen J E 1992 *Phys. Scr.* **45** 497

Allen J E, Annaratone B M and de Angelis U 2000 *J. Plasma Phys.* **63** 299

[28] Kersten H, Stoffels E, Stoffels W W, Otte M, Csambal C, Deutsch H and Hippler R 2000 *J. Appl. Phys.* **87** 3637

[29] Bronold F X, Fehske H, Kersten H and Deutsch H 2008 *Phys. Rev. Lett.* **101** 175002

[30] www.asiinstruments.com/technical.aspx

[31] Khrapak S A *et al* 2005 *Phys. Rev.* E **72** 016406

[32] Daugherty J E, Porteous R K and Graves D B 1993 *J. Appl. Phys.* **73** 1617

[33] Trottenberg Th, Kersten H and Neumann H 2008 *New J. Phys.* **10** 063012

[34] Demtröder W 2006 *Experimentalphysik, Band 1: Mechanik und Wärme* 4th edn chapter 8 (Berlin: Springer)

[35] Rader D J 1990 *J. Aerosol. Sci.* **21** 161

[36] Cunningham E 1910 *Proc. R. Soc.* A **83** 357

[37] Millikan R A 1911 *Phys. Rev.* **32** 366

[38] Epstein P S 1924 *Phys. Rev.* **23** 710–33

[39] Nitter T 1996 *Plasma Sources Sci. Technol.* **5** 93–111

[40] Kersten H, Deutsch H, Steffen H, Kroesen G M W and Hippler R 2001 *Vacuum* **63** 385

[41] Hippler R 2008 Elementary processes of plasma surface interactions *Low Temperature Plasmas* vol 1 ed R Hippler, H Kersten, M Schmidt and K H Schoenbach (Berlin: Wiley) pp 71

[42] Riemann K-U 1991 *J. Phys.D: Appl. Phys.* **24** 493